Interaction Chamber Design for an Energy Continuously Tunable Sub-Mev Laser-Compton Gamma-Ray Source

Hanghua Xu, Gongtao Fan, Hailong Wu, Jianhui Chen, Benji Xu, Wang Xu, and Dong Wang

***Abstract*—Previously, fixed angle Laser-Compton Scattering (LCS) experiments have been conducted at the terminal of the 100 MeV LINAC of the Shanghai Institute of Applied Physics, using SINAP-I and SINAP-II facility. Sub-MeV energy continuously tunable laser-Compton light source device (SINAP-III) is an updated facility that will allow the collision angle between the laser and electron beam continuously adjustable from 20° to 160°. This new feature will enable convenient control on the maximum energy of the generated X/γ ray in a wide energy region, especially when the energy of electrons cannot be momentarily adjusted, e.g. on the storage ring. Keeping the electron beam and laser beam waist coincident at arbitrary angle is crucial for LCS gamma-ray production, an interaction chamber containing a rotatable bracket that holds a series of plane mirrors and convex lens is presented. This work is a summary of its design. The simulation of photon production's variation caused by the systematic errors is performed using a MC code. The accuracies of installation and adjustment of mirrors and lens are given according to the simulation results. The sizes of these optical devices are also optimized.**

***Index Terms*—Compton scattering, energy resolution, gamma rays, instrumentation, particle collisions, photon beams.**

I. Introduction

In THE past ten years, with the development of advanced accelerator and laser technology, the new X/γ-ray source based on Compton scattering made rapid progress and was rated as one of the most potential in the field of ultra- short pulse light sources. It uses high-power, short-pulse laser beam and high brightness, relativistic electron beam to achieve Compton scattering which produces high flux, short-pulse, quasi-monochromatic X/γ-rays. Currently, many research institutions such as LLNL [1], BNL [2], [3], SLAC [4], IAC [5], MIT [6], Spring8 [7], [14], JAEA [8], ESRF [9], INFN [10] and TUNL [11] are committed to the construction and development of the experimental device of LCS. The produced X/γ-rays have wide applications in nuclear physics, medical, energy, defence and industrial applications. The energy of the scattered X/γ-ray photon [9], [12] is

$$E_x = E_L \frac{(1-\beta\cos\theta)}{1-\beta\cos\theta_S + \frac{E_L}{E_e}[1-\cos(\theta-\theta_S)]} \quad (1)$$

where β is the electron velocity normalized to the speed of light, E_e and E_L are the energies of the incident electron and laser photon, and θ and θ_S are the incident angle of the laser photon and the angle of the scattered X/γ ray with respect to the direction of the incident electron beam. Through this equation, we can see that the energy of X/γ ray can be tuned by either change of these four variables. From the current view of existing devices and proposals, LCS X/γ rays are generally produced in backscattering geometry, i.e. fixing θ to 180°. In these cases, the energy of X/γ rays are usually varied by changing E_e or E_L in existing LCS facilities.

Changing the wavelength of laser has two limitations: first, the wavelength of laser cannot be changed continuously in a wide range, usually the variation of wavelength is achieved by switching laser devices. Some optical components along the laser transportation path such as quarter-wave plate, lens have to be switched, too. This will take some time to adjust the laser pulse at the interaction position to the desired status.

Changing the electron's energy is not suitable for LCS based on the storage ring when the ring serves not only for the LCS experiment, but also operating other beam lines that require a stable electron energy.

Tuning the energy of X/γ ray by changing θ_S using a collimator-absorber system is simulated in [13], showing that it is not suitable for experiments if quasi-monochromatic X/γ ray of small spot size is essential. This method is inappropriate when the scattered photon's energy reaches over hundreds of MeV, since the collimator have to be very thick and pair creation effect is not negligible.

Tuning the energy of X/γ ray by continuously changing the incident angles of the laser can avoid the problems mentioned above. Combined with proper collimator or tagger [14], this method can produce X/γ ray with high energy resolution either on linac or on storage ring. Fig. 1 show a simulated result of change of the energy spectra of the scattered photons caused

Manuscript received May 26, 2015; revised July 24, 2015; accepted September 24, 2015. Date of publication January 04, 2016; date of current version April 15, 2016. This work was supported by the Chinese Academy of Science under Grant YZ201246.

H. Xu and H. Wu are with the Free Electron Laser Department, Shanghai Institute of Applied Physics, Shanghai 100049, China and also with the University of Chinese Academy of Sciences, Beijing 100049, China.

G. Fan and B. Xu are with the Nuclear Physics Department, Shanghai Institute of Applied Physics, Shanghai 100049, China (e-mail: fangongtao@sinap.ac.cn).

J. Chen and D. Wang are with the Free Electron Laser Department, Shanghai Institute of Applied Physics, Shanghai 100049, China.

W. Xu was with the Nuclear Physics Department, Shanghai Institute of Applied Physics, Shanghai 100049, China.

Color versions of one or more of the figures in this paper are available online at http://ieeexplore.ieee.org.

Digital Object Identifier 10.1109/TNS.2015.2496256

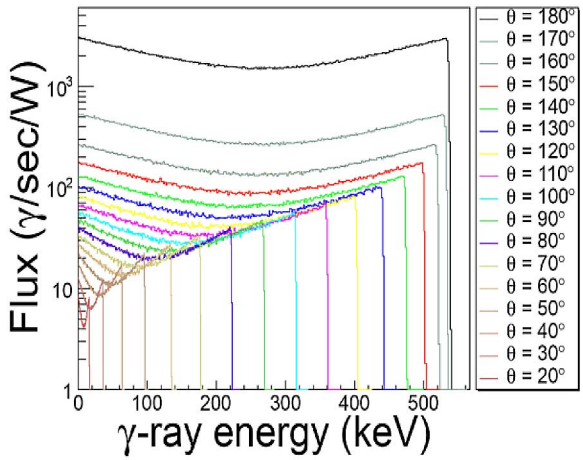

Fig. 1. Change of the energy spectra of the scattered photons caused by variation of incident angle by simulation. The wavelength of the laser is 800 nm, and the energy of electrons is 150 MeV.

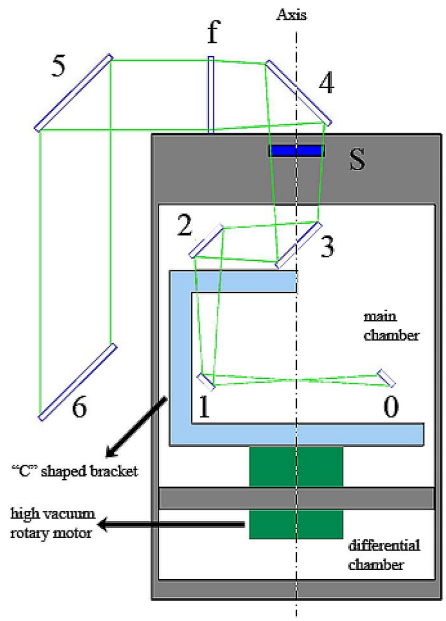

Fig. 2. Scheme diagram of the basic transportation structure (side view). The rectangles with number 0-6 represent plane mirrors, the rectangle referring to "f" is a convex lens, and the one with "s" is a transparent glass which is on the top of the chamber. The dash dot line is the axis of the whole cylindrical chamber.

by variation of the incident angle. As shown in Fig. 1, the larger the incident angle of laser, the higher both the total flux and the maximum energy of scattered X/γ ray.

It is worth to mention the disadvantages of this method that the decrease of the incident angle will reduce the degree of polarization of the X/γ ray.

Based on the technological accumulation from fixed angle LCS experiments, i.e. SINAP-I [15] and SINAP-II [12], SINAP-III facility [16] as an energy continuously tunable sub-MeV gamma-ray source based on Laser Compton scattering is proposed. It will be constructed on the branch line of Shanghai Deep-Ultraviolet Free-Electron Laser (SDUV-FEL) [17]. The electrons and laser are both imported from into an interaction chamber. A specially designed laser transport system enables θ to be continuously changed from 20° to 160°, scattered photon energy E_x is thus continuously adjustable easily without changing E_e and E_L.

Different from conventional methods, the main challenges of our experiment are: 1) keeping the electron beam bunch and laser beam waist overlap at interaction point within tens of microns at arbitrary colliding angles; 2) synchronizing the laser pulse and the electron pulse within picosecond at interaction point.

In this paper, we present the optical design of the interaction chamber to solve these two problems. The design of chamber's laser transport system and the adjustment devices built to regulate the laser propagation are demonstrated first. The detecting components and alignment scheme are summarized in the second part. A study on the optimization of the sizes of chamber and mirrors and the tolerance of mirrors are illustrated as the third part.

II. Laser Transport System

To achieve the continuous adjustability of the colliding angle of the electron beam and laser beam, an array of mirror and lens with several adjustment devices is designed.

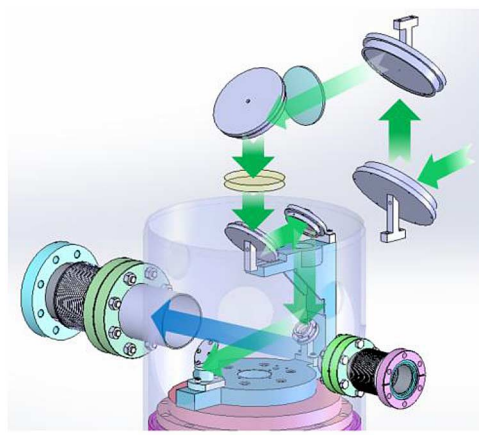

Fig. 3. A 3D view of the basic transportation structure. The blue arrows show the way that electron bunch goes and the green arrows show the way that laser goes.

A. Basic Structure

As shown in Fig. 2, laser beam would propagate along the path from mirror No.6 to mirror No.0. The green lines in Fig. 2 is the maximum envelope of laser beam that these optical elements' apertures can hold.

Mirror No.4-6 and convex lens f are placed in the atmosphere, while mirror No.0-3 are set inside the vacuum chamber on the "C" shaped bracket. Laser beam is expected to be focused at the centre of mirror No.1 and mirror No.0, colliding with electron bunches that come across the chamber through bellows, as shown in Fig. 3, and the produced X/γ-rays will come outside, along with the electron beam's incident direction.

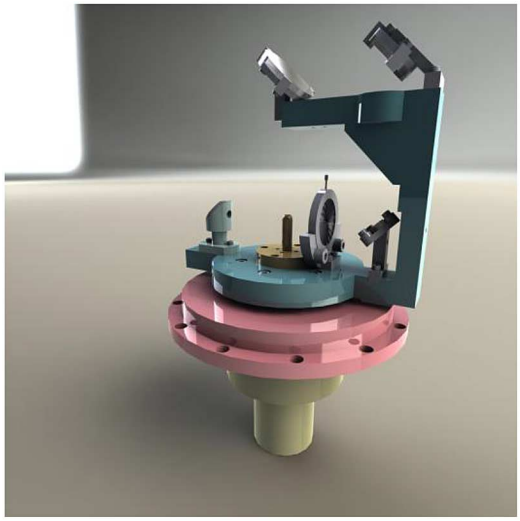

Fig. 4. A 3D view of the rotatable bracket holding mirrors No.0-3.

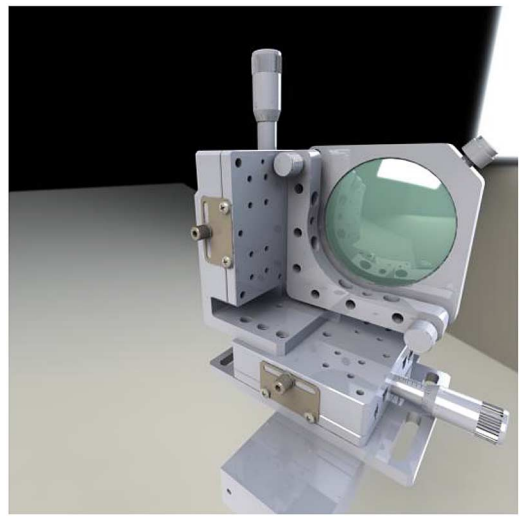

Fig. 5. A 3D view of translation device of convex.

A 3D view of the designed rotatable bracket holding mirror No.0-3 is shown in Fig. 4.

The design idea contained in this arrangement of mirror is clear and straightforward.

Since the laser beam is expected to turn a large angle of 140° continuously, injection from side face of chamber is not suitable. Rather than hoping for the creation of a large and flawless arc glass that will have slight deformation under baking and influence little on the focusing, we decide to move the rotation part inside vacuum chamber to avoid these problems. But the laser still needs an entrance, so we chose to set a flange on the top of the chamber. Laser will shoot on the top glass normally. The change of laser waist caused by diffraction, thermal expansion and deformation from pressure is negligible in this geometry.

The rotation of laser beam is realized by revolving mirror No.1 and No.0 around the axis of the chamber. The electron beam is obviously set to shoot at the crossing point of the axis of the chamber and the laser path between mirror No.1 and No.0. Then mirror No.2 and mirror No.3 are added to the design to connect the light path of the rotating part to the entrance.

Mirror No.4 and lens f is set outside the chamber. They can be replaced by an off-axis parabolic mirror, but we still chose to use a mirror and a convex lens considering several reasons. First, the power of our laser is not very high, the energy of each pulse is about 3.5 mJ, and the pulse length is 1 ps (rms). So the dispersion effect can be neglected. Second, it is not difficult to find out that coincidence of the chamber's axis and the laser path's axis between mirror No.4 and No.3 is very important in our design. Parallel or angular deviation will both cause laser waist's shift during rotation. Mirror No.4 and convex lens f can adjust the laser separately to achieve best coaxial status while off-axis parabolic mirror would cause the unwilling coupled adjustment.

Mirror No.5 and No.6 are used to transport the incoming expanded laser to the convex lens.

B. Adjustment Devices

In order to control waist position, we set up several remote control devices on the basic optical path.

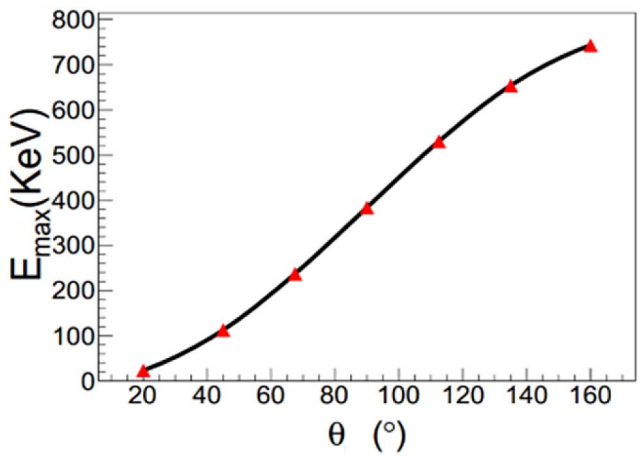

Fig. 6. The relationship between the incident angle and the maximum energy of scattered photon when the wavelength of the laser is 800 nm, and the energy of electrons is 180 MeV.

A two dimensional frame combined with linear stages shown in Fig. 5 is designed to hold and adjust the convex lens. This device can make translation of the lens's position.

Another similar device is set up for mirror No.4, but the linear stage is replaced with a piezoelectric ceramic driven flexible micro positioning platform, which can make a careful adjustment of the orientation of mirror No.4.

The continuous change of incident angle of laser is realized by the rotation of the bracket. The relationship between the incident angle and the maximum energy of the scattered photon is shown in Fig. 6.

As shown in Fig. 7, the smaller the incident angle θ, the greater the relative change of maximum energy caused by θ's variation. If we want to tune the maximum energy at a resolution of 1/1000, the minimum step of θ's adjustment must be less than 0.01°.

In order to realize this precise control of incident angle, the bracket holding mirrors is driven by an ultra-high vacuum motor which is set up in the differential chamber under the main chamber. And the circular grating ruler is used to measure

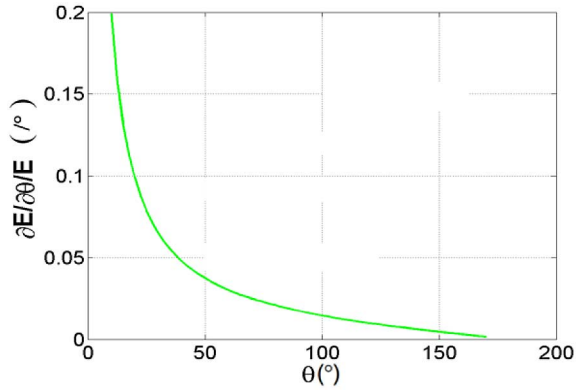

Fig. 7. Relationship between $(\partial \mathrm{E}/\partial\theta)/\mathrm{E}$ and θ.

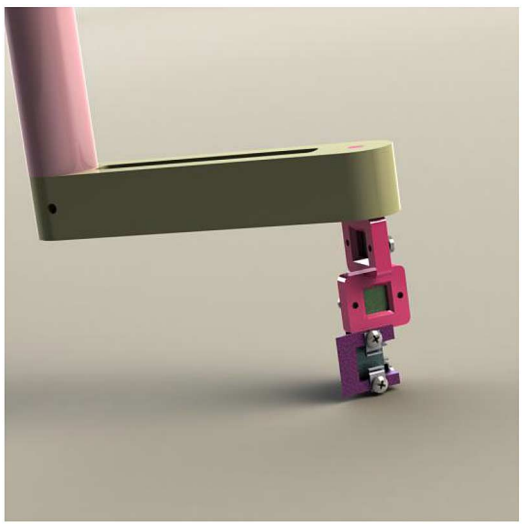

Fig. 8. A 3D view of lifting bracket for fluorescent target.

the angle of rotation accurately. The differential chamber is set to prevent the drop of vacuum degree in the main vacuum chamber caused by the operation of the high vacuum motor.

III. Observation Devices and Alignment Scheme

Only adjustment devices is not enough to perform the whole alignment process. Fluorescent target, cameras, photodetector (PD) are used as observation devices to help measuring the deviation of the laser from the interaction point (IP) in transverse and longitudinal directions.

A. Coarse Spatial Overlap

The interaction point is observed and measured by inserting fluorescent target. The target films is fixed on a lifting bracket, as shown in Fig. 8. Both the spot of laser and fluorescence caused by electron bunches will be shot through the observation windows by cameras, offering feedback to the remote control devices.

The accuracy of this method depends on the resolution of fluorescent target films which is expected to be 100 μm.

B. Coarse Temporal Synchronization

The temporal synchronization adjustment between the laser and the electron beam is accomplished in several steps.

A general synchronization method is adopted based on the synchronizing system of the SDUV-FEL. A drive laser of 266 nm wavelength is used to shoot at photocathode to produce electrons for Compton scattering. Another beam of laser with the wavelength of 800 nm is used as the incident laser in Compton scattering. By adjusting the trigger of the incident laser and the drive laser, the interval of the electron and the incident laser beam's arrival time can be adjusted within several nanoseconds. The arrival time of the electron beam and the laser could be determined by the photo-dipole (PD) outside the chamber by detecting the synchrotron radiation (SR) signal of the electron beam and the laser simultaneously. The SR signal and the laser beam are reflected outside the vacuum chamber by an optical transition radiation (OTR) screen and then focused into the PD. The oscilloscope will capture the two signals detected by the PD. One can adjust the RF reference phase of the laser to make the two signals showed by the oscilloscope exactly at the same position. By using a fast 2 GHz PD and a high resolution oscilloscope with 6 GHz bandwidth and 25 GS/s sampling rate, the electron beam and the seed laser could be temporally overlapped with a precision better than 50 ps.

C. Fine Alignment

Final precise alignment is achieved by monitoring the flux of the scattered photons using the detector while tuning the seed laser delay precisely and changing the position of laser waist.

When the collision event does not occur, only the background signal could be observed in the detector, and the energy spectrum is rather flat. While one adjusts the laser delay with femtosecond level precision in the right direction, a peak should be expected. The faster growing speed of the peak in the spectra reaches, the better alignment is achieved.

IV. Optimization and Tolerance Study of Mirrors

Next, in order to specify the accuracies of installation and adjustment of mirrors and lens, the simulation of photon production's variation caused by the systematic errors is performed using a MC [18] code.

The main parameter used in simulation is listed in Table I.

A. Optimization of Mirrors' Sizes and Positions

To decide the mirrors' tolerance, the size and position of mirrors which is constrained by the waist radius of laser have to be obtained first.

The flux of gamma-ray is simulated with the laser beam radius σ_{p} (σ_{wp} is set to be equal to σ_{hp}, so we use σ_{p} for simplicity) set from 5 μm to 320 μm and the incident angle set from 20° to 160°, as shown in Fig. 9. We can see that the waist radius of laser reaches about 2 times of the radius of the electron beam when gamma-ray's flux is decreased by approximately half. The target flux of the gamma-rays in SINAP-III is $10^4 - 10^6$ photons/collision. So the max laser waist radius should be less than 40 μm to achieve an acceptable flux.

Then, we perform an optimization on the mirror size and position using the laser waist radius. When the laser waist radius is fixed, the mirror size is mainly affected by its position. As shown in Fig. 2, the laser's envelope grows rapidly as the mirror

TABLE I
SIMULATION PARAMETERS

Electron in Linear accelerator	
Electron energy (MeV)	150
Energy spread	(%)0.1
Normalized emittance (mm•mrad)	6
Bunch length (rms) (σ_{le}) (mm)	0.72
RMS beamsize (σ_{we}/σ_{he}) (μm)	20/20
Ti:Sa laser	
Laser wavelength (nm)	800
Energy/pulse (mJ)	1.75
Repetition rate (Hz)	1000
Pulse length (rms) (σ_{lp})	1ps
RMS waistsize (σ_{wp}/σ_{hp}) (μm)	20/20
Incident angle (°)	20-160

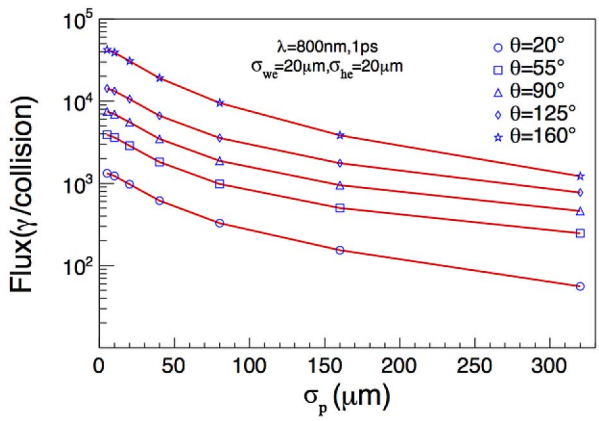

Fig. 9. Flux of gamma ray changed caused by waist radius.

moves away from the waist of the laser. The mirror size is optimized to be as small as possible to avoid the disadvantage caused by larger mirror size, e.g. bending, unevenness, larger space cost which means an ion pump of greater pumping speed need to be applied.

The whole optimization process is complicated and involves a lot of geometric calculation. Briefly speaking, on one hand, if the No.1 mirror get too close to the interaction point, it will be easy to block the electron beam, and the rotation range of the "C" shaped bracket will be less than 140°. On the other hand, if the No.1 mirror get too far away from the interaction point, the mirrors' sizes would be too large, and the chamber would be unable to contain the mirrors. So there exists an optimized configuration.

By setting a series of constraint conditions shown in Table II, we obtain the results as shown in the Fig. 10, where the vertical axis is the distance from mirror No. 1's center to IP, and the horizontal axis is the inner radius of the interaction chamber. The red area indicates that the constraint conditions are satisfied, the blue area is the infeasible region. We need the smallest chamber and the lens and mirrors, so the left lower corner of the red area is what we want. In order to facilitate processing, we adjust the optimized diameters of mirrors to be either divisible by 5 or close to the value of the diameters of standard flanges.

The results are collected in Table III. In order to have larger mirrors to maintain high energy transfer rate when laser beam

TABLE II
MAIN CONSTRAINT CONDITIONS

No.1	Mirrors No.2 and No.3 are not interfered with chamber
No.2	Electron beam is not blocked by Mirror No.1's edge when incident angle is 20° or 160°
No.3	The diameter of mirror No.6 is less than 100mm

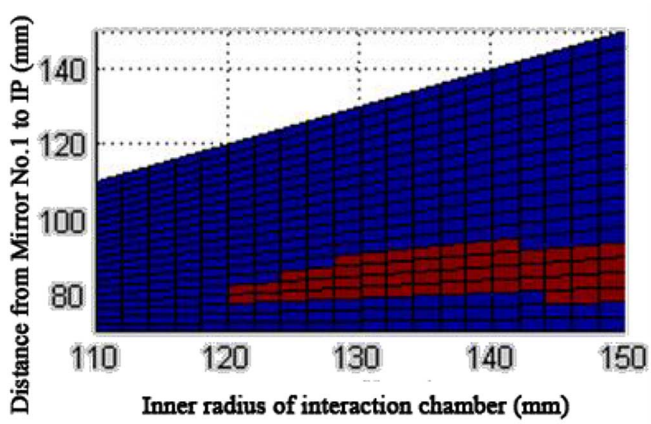

Fig. 10. Chamber radius minimization result.

TABLE III
OPTIMIZED MIRRORS' SIZE AND POSITIONS

Mirror's No	Thickness (mm)	Diameter (mm)	Horizontal distance from IP to the mirror's centre (mm)	Vertical distance from IP to the mirror's centre (mm)
1	5	18	80	0
2	5	40	80	125
3	5	55	0	125
4	10	80	0	290
5	10	95	240	290
6	10	95	240	150
0	5	18	80	0
f	6	70	80	290
s	10	63	0	200

propagate along non ideal path due to tolerances and other factors, we use the laser radius of 20 μm rather than 40 μm as input.

B. *Tolerance of Mirrors' Installation and Adjustment*

The deviation of waist position of the laser beam from the best interacting point is also analyzed. The drop of gamma-ray flux caused by deviation in the horizontal direction is shown in Fig. 11. It is caused by the decrease of average density of electrons and photons in the effective interaction region resulted from the deviation of the laser pulse from the electron bunch.

Similar to the requirement of waist radius, the half decrease is set as the threshold, we obtain the allowed waist position deviation (shown in Table III), which are exactly the upper limits of the cumulative errors of installation and adjustment of mirrors and lens.

Δx, Δy, Δz are referring to the deviation of the waist position in horizontal, vertical and laser propagation directions respectively, as shown in Fig. 12.

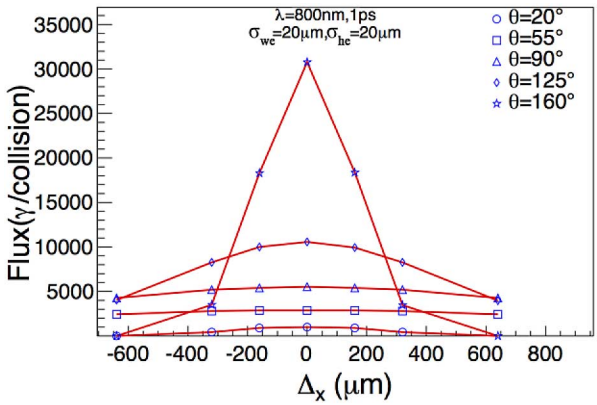

Fig. 11. Flux change of gamma ray caused by Δx.

TABLE IV
ALLOWED WAIST POSITION DEVIATIONS

Δx (μm)	200
Δy (μm)	30
Δz (μm)	800

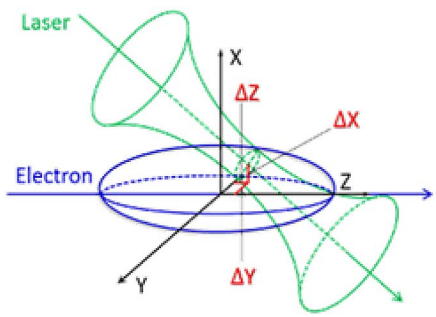

Fig. 12. Schematic diagram showing the deviation of laser waist centre from the centre of electron bunch.

V. CONCLUSION

Tuning energy continuously and precisely in a wide range is one of the LCS light source's developing trends. And the continuous change of the angle between the laser and the electron is one of the most effective methods to realize it.

In this paper, we present a design of an interaction chamber to achieve continuous and precise adjustment of the angle between the electron beam and laser beam in laser Compton scattering. This feature will enable convenient control on the maximum energy of the generated X/γ ray.

The chamber will be installed as the core component of SINAP III. The design of this interaction chamber can be applied to other LCS light sources that want to have a wide energy range and about 1‰ energy resolution at the same time. It may be of great referential significance for the construction of LCS light source in the future.

ACKNOWLEDGMENT

The authors would like to acknowledge Yalan Han and Weihua Li for helping them draw the engineering chart. They also thank Xingtao Wang, Bo Liu, Xiangchun Shi, and Jinyue Liu for their helpful discussions.

REFERENCES

[1] D. J. Gibson, S. G. Anderson, C. P. J. Barty, S. M. Betts, R. Booth, W. J. Brown, J. K. Crane, R. R. Cross, D. N. Fittinghoff, F. V. Hartemann, J. Kuba, G. P. L. Sage, D. R. Slaughter, A. M. Tremaine, A. J. Wootton, E. P. Hartouni, P. T. Springer, and J. B. Rosenzweig, "Pleiades: A picosecond Compton scattering x-ray source for advanced backlighting and time-resolved material studies," *Phys. Plasmas*, vol. 11, pp. 2857–2864, 2004.

[2] A. M. Sandorfi, M. J. Le Vine, C. E. Thorn, G. Giordano, G. Matone, and C. Schaerf, "High energy gamma ray beams from Compton backscattered laser light," *IEEE Trans. Nucl. Sci.*, vol. 30, no. 4, pp. 3083–3087, Aug. 1983.

[3] I. V. Pogorelsky, I. B. Zvi, T. Hirose, S. Kashiwagi, V. Yakimenko, K. Kusche, P. Siddons, J. Skaritka, T. Kumita, A. Tsunemi, T. Omori, J. Urakawa, M. Washio, K. Yokoya, T. Okugi, Y. Liu, P. He, and D. Cline, "Demonstration of photons/second peaked at 1.8 A in a relativistic Thomson scattering experiment," *Phys. Rev. Special Topics–Accel. Beams*, vol. 3, pp. 090702–1, 2000.

[4] C. Bula, K. T. McDonald, E. J. Prebys, C. Bamber, S. Boege, T. Kotseroglou, A. C. Melissinos, D. D. Meyerhofer, W. Ragg, D. L. Burke, R. C. Field, G. Horton. Smith, A. C. Odian, J. E. Spencer, D. Walz, S. C. Berridge, W. M. Bugg, K. Shmakov, and A. W. Weidemann, "Observation of nonlinear effects in Compton scattering," *Phys. Rev. Lett.*, vol. 76, pp. 3116–3119, Apr. 1996.

[5] K. Chouffani, D. Wells, F. Harmon, G. Lancaster, and J. Jones, "Laser-Compton scattering as a potential bright x-ray source," JCPDS-International Centre for Diffraction Data 2003, Advances in X-ray Analysis, vol. 46, pp. 74–79, 2002.

[6] W. S. Graves, J. Bessuille, P. Brown, S. Carbajo, V. Dolgashev, K. H. Hong, E. Ihloff, B. Khaykovich, H. Lin, K. Murari, E. A. Nanni, G. Resta, S. Tantawi, L. E. Zapata, F. X. Kartner, and D. E. Moncton, "Compton x-ray source based on burst-mode inverse Compton scattering at 100 kHz," *Phys. Rev. ST. Accel. Beams*, vol. 17, p. 120701, 2014.

[7] M. Niiyama, "Recent results from LEPS and prospects of LEPS II at SPring-8," *Nucl. Phys. A*, vol. 914, pp. 543–552, 2013.

[8] R. Hajima, "Generaton of laser Compton scattered gammy-rays from a 150-Mev microtron," in *Proc. IPAC*, Shanghai, China, 2013, pp. 3645–3647 [Online]. Available: http://accelconf.web.cern.ch/AccelConf/IPAC2013/papers/thpwa009.pdf

[9] A. D. Angelo, O. Bartalini, V. Bellini, P. L. Sandri, D. Moricciani, L. Nicoletti, and A. Zucchiatti, "Generation of Compton backscattering γ-ray beams," *Nucl. Instrum. Methods Phys. Res. A*, vol. 455, pp. 1–6, 2000.

[10] D. Alesini, I. Chaikovska, A. Variola, S. Guiducci, F. Zomer, C. Milardi, and M. Zobov, "DAΦNE gamma-rays factory," e-Print Arxiv:1405.0861 2014.

[11] H. R. Weller, M. W. Ahmed, H. Gao, W. Tornow, Y. K. Wu, M. Gai, and R. Miskimen, "Research opportunities at the upgraded HIgS facility," *Prog. Part. Nucl. Phys.*, vol. 62, pp. 257–303, 2009.

[12] W. Luo, W. Xu, Q. Y. Pan, X. Z. Cai, J. G. chen, Y. Z. Chen, G. T. Fan, G. W. Fan, W. Guo, Y. J. Li, W. H. Liu, G. Q. Lin, Y. G. Ma, W. Q. Shen, X. C. Shi, B. J. Xu, J. Q. Xu, H. O. Zhang, Z. Yan, L. F. Yang, and M. H. Zhao, "A laser-Compton scattering prototype experiment at 100 Mev linac of shanghai institute of applied physics," *Rev. Sci. Instrum.*, vol. 81, p. 013304, 2010.

[13] H. Ohgaki, S. Koda, Y. Iwasaki, Y. Takabayashi, K. Yoshida, T. Tomimasu, Y. Uozumi, and K. Ishibashi, "Study on eenergy variable laser-Compton gamma-ray with a fixed energy electron beam," *J. Nucl. Sci. Technol.*, vol. 44, no. 5, pp. 698–702, 2007.

[14] N. Muramatsu, Y. Kon, S. Date, Y. Ohashi, H. Akimune, J. Y. Chen, M. Fujiwara, S. Hasegawa, T. Hotta, T. Ishikawa, T. Iwata, Y. Kato, H. Kohri, T. Matsumura, T. Mibe, Y. Miyachi, Y. Morino, T. Nakano, Y. Nakatsugawa, H. Ohkuma, T. Ohta, M. Oka, T. Sawada, A. Wakai, K. Yonehara, C. J. Yoon, T. Yorita, and M. Yosoi, "Development of high intensity laser-electron photon beams up to 2.9 GeV at the spring-8 LEPS beamline," *Nucl. Instrum. Methods Phys. Res. A*, vol. 737, pp. 184–194, Feb. 2014.

[15] W. Luo, W. Xu, Q. Y. Pan, X. Z. Cai, Y. Z. Chen, G. T. Fan, G. W. Fan, J. Li, W. H. Liu, G. Q. Lin, Y. G. Ma, W. Q. Shen, X. C. Shi, B. J. Xu, J. Q. Xu, Y. Xu, H. O. Zhang, Z. Yan, L. F. Yang, and M. H. Zhao, "X-ray generation from slanting laser-Compton scattering for future energy-tunable shanghai laser electron gamma source," *Appl. Phys. B*, vol. 101, pp. 761–771, 2010.

[16] W. Xu, W. Luo, B. S. Huang, Z. D. An, Y. J. Li, L. F. Yang, G. T. Fan, Z. Yan, B. J. Ben, X. L. Cai, Q. Y. Pan, and G. W. Fan, "Adjustable LCS γ source SINAP-III," *Nucl. Phys. Rev.*, vol. 29, no. 3, pp. 253–258, 2012.

[17] H. X. Deng and C. Feng, "Using off-resonance laser modulation for beam-energy-spread cooling in generation of short-wavelength radiation," *Phys. Rev. Lett.*, vol. 111, p. 084801, Aug. 2013.

[18] W. Luo, W. Xu, Q. Y. Pan, Z. D. An, X. L. Cai, G. T. Fan, G. W. Fan, Y. J. Li, B. J. Xu, Z. Yan, and L. F. Yang, "A 4D monte carlo laser-Compton scattering simulation code for the characterization of the future energy-tunable SLEGS," *Nucl. Instrum. Methods Phys. Res. A*, vol. 660, no. 1, pp. 108–115, Dec. 2011.